Investigating the Orbital Dynamics of Mercury

Alex Boxer, Oliver Blease, Shreya Ghosh, Carolena Lukaszek, Thomas Mansfield, Harry Nsubuga

November 8, 2024

Abstract

This report explores different numerical methods to model the orbit of Mercury. Introducing Kepler's laws as a basis for our understanding. We proceed to use Python to model Kepler's law and visualise the plots, deriving initial conditions to map them onto our code. We analyse and compare our data with the observed values found by NASA, extending the model to concepts of General Relativity and Chaos to demonstrate a modern understanding of orbital dynamics. Concluding with a difficulties faced section, given a limited time-frame.

1 Mathematical Background

1.1 Kepler's Laws

Kepler's laws describe the motion of planets around the Sun, stating that orbits are elliptical, areas are swept out equally in equal times, and orbital periods relate to the semi-major axis by a specific mathematical ratio.

1.1.1 1st: Law of orbits

Each planet orbits the Sun in an elliptical path, with the Sun positioned at one of the ellipse's focal points. As the planet travels along this elliptical orbit, its distance from the Sun varies, changing as it moves through different points in its path.

1.1.2 2nd: Law of areas

As a planet orbits the Sun, an imaginary line connecting the planet to the Sun sweeps out equal areas in equal time intervals. This means that planets don't maintain a constant speed in their orbits. Instead, they adjust their speed to cover equal areas in the same amount of time: moving faster when closer to the Sun and vice versa. The closest point in a planet's orbit to the Sun is known as *perihelion*, while the farthest point is *aphelion*. According to Kepler's second law, a planet reaches its maximum speed at perihelion and its minimum at aphelion.

1.1.3 3rd: Law of periods

The square of a planet's orbital period is directly proportional to the cube of the semi-major axis of its orbit, such as:

$$T^2 = a^3, \tag{1.1}$$

where T is the orbital period and a is the semi-major axis. This implies that as a planet's distance from the Sun increases, the time required to complete one orbit increases further. Earth taking 365 days to orbit the Sun, Mercury takes 88 days, whereas Saturn requires 10,759 days [1].

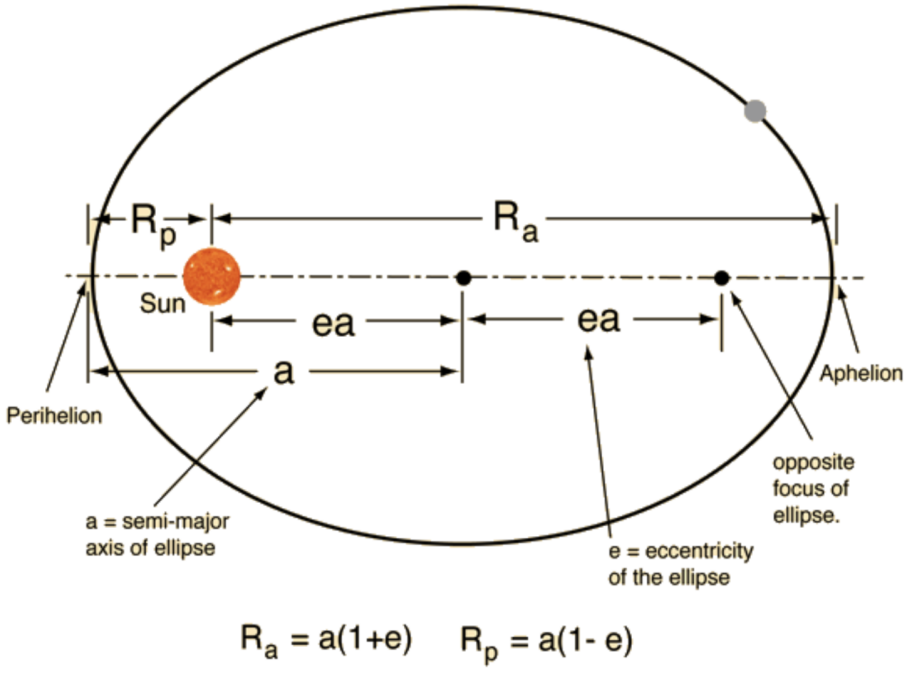

Figure 1: Diagram of Kepler's Laws showing the elliptical orbit of a planet around the Sun, with points such as perihelion and aphelion. As found in [2].

1.2 Newtonian Understanding

Newton formulated the law of gravitation from Kepler's 3rd law. It can be derived by considering two bodies of masses m_1 and m_2, orbiting their (stationary) centre of mass at distances r_1 and r_2 (Figure 2).

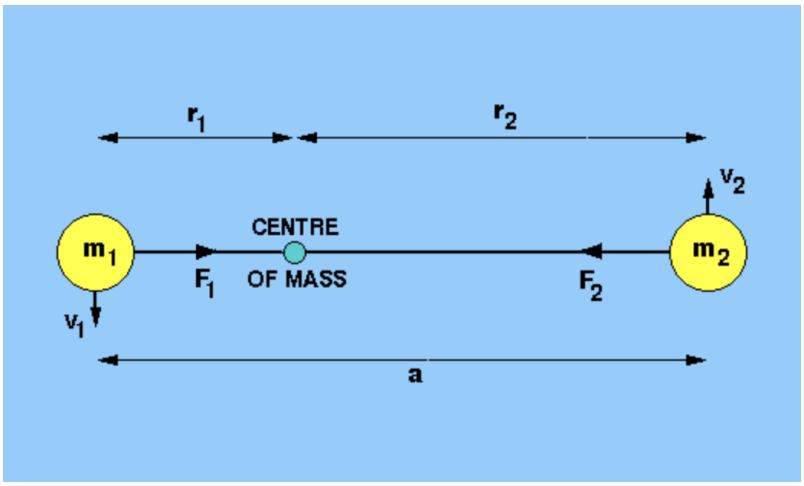

Figure 2: Two bodies in orbit about their common centre of mass. As found in [3].

Since the gravitational force acts along the line joining the centres of the bodies, both bodies must complete one orbit in the same period T (though they move at different speeds v_1 and v_2). The forces on each body due to their centripetal accelerations are therefore:

$$F_1 = \frac{m_1 v_1^2}{r_1} = \frac{4\pi^2 m_1 r_1}{T^2}.$$

$$F_2 = \frac{m_2 v_2^2}{r_2} = \frac{4\pi^2 m_2 r_2}{T^2}.$$

By Newton's third law, $F_1 = F_2$, and so

$$\frac{r_1}{r_2} = \frac{m_2}{m_1}$$

this implies that the more massive body orbits closer to the centre of mass than the less massive body. The total separation of the two bodies is given by

$$a = r_1 + r_2,$$

which gives

$$r_1 = \frac{m_2 a}{m_1 + m_2}.$$

Combining this equation with the expression for F_1 derived above and Newton's law of gravitation ($F_{\text{grav}} = F_1 = F_2 = \frac{Gm_1m_2}{a^2}$) gives Newton's form of Kepler's third law:

$$T^2 = \frac{4\pi^2 a^3}{G(m_1 + m_2)}. \tag{1.2}$$

1.2.1 Energy Conservation

The total energy of an orbiting body remains constant, due to the absence of any non-conservative forces, and the conservation of energy law applies. Objects moving in a gravitational field (in this case we use the example of Mercury orbiting the Sun) will have two energies attributed to it if no other forces are acting upon it, the gravitational potential and kinetic energy. We start by defining the radius of minimum curvature:

$$R = a(1 - e^2) \tag{1.3}$$

and the distance between the two bodies at the aphelion:

$$r = (1 - e)a. \tag{1.4}$$

From Newton's Laws of Gravitation and the centripetal force equation:

$$\frac{mv^2}{R} = \frac{GmM}{r^2}. \tag{1.5}$$

Since kinetic energy is $KE = \frac{1}{2}mv^2$ we can rearrange the equation, multiply by one half and substitute the values of R and r to give the kinetic energy as

$$KE = \frac{GmM(1 + e)}{2(1 - e)a}, \tag{1.6}$$

the potential energy can also be derived as

$$PE = -\int F\dot{d}r = GMm \int \frac{1}{r^2} dr = -\frac{GMm}{r} = -\frac{GmM}{(1 - e)a}. \tag{1.7}$$

From the conservation of energy, $E = KE + PE$, we get that

$$E = -\frac{GmM}{2a} \tag{1.8}$$

which is a constant thus confirming that an orbital system does obey the laws of conservation of energy.

1.3 Astronomical Units

When working on problems at an astronomical scale, the use of SI units results in very large numbers, making calculations difficult. To simplify this, we use *astronomical units (AU)*.

The astronomical unit is defined as the average distance between the Earth and the Sun:

$$1\,\text{AU} = 1.496 \times 10^{11}\,\text{m}.$$

In these units, the mass of the Sun (*solar mass*) ($M_\odot$) and the orbital period (T) of planets around the Sun (measured in years) allow us to work with Newton's law of gravitation and Kepler's third law with less hassle.

Starting from 1.2 , for $m_1 \gg m_2$, the orbital period of a planet is given by:

$$T^2 = \frac{4\pi^2 a^3}{G m_1}, \tag{1.9}$$

In the context of our problem:

- The central body is the Sun, so $m_1 = M_\odot$,
- T is the orbital period (in years),
- a is the semi-major axis of the orbit (in AU).

Using Kepler's third law (1.1), we can solve for G in these units. By substituting $T = 1\,\text{yr}$, $a = 1\,\text{AU}$, and $m_1 = M_\odot$, we obtain:

$$G = \frac{4\pi^2\,(1\,\text{AU})^3}{M_\odot\,(1\,\text{yr})^2}. \tag{1.10}$$

Here: G is expressed in units of $\text{AU}^3\,\text{yr}^{-2}\,M_\odot^{-1}$. Equating the units to 1 in our code.

1.4 General Relativity

It soon became evident that Newtons models for modelling the planetary bodies did not give a fully accurate picture of the universe. For example: his theory predicted Mercury would have a largely stable orbit, however later observations demonstrated Mercury's perihelion processed around the Sun 43 arcseconds per century faster than Newton's models had predicted. Newton's models also failed to account for the light deflection around massive objects that astronomers had began to observe. Deflections that were at least double what was predicted by Newton's models around massive objects like the Sun. These issues clearly demonstrated a new model was needed to account for these discrepancies. This came in the form of *Einstein's Theory of General Relativity*. His theory involved generalising his earlier theory of Special Relativity and refining Newton's Theory of Gravitation to describe gravity as a geometric property of four dimensional space-time, rather than as a force.

This theory was able to account for Mercury's perihelion advance by introducing a correction term to Newton's gravitation formula of the form:

$$-\frac{3mM^2G^2}{2c^2r^3}\vec{r}. \tag{1.11}$$

This correction can be derived from the first and most basic non-trivial solution to Einstein's general relativity field equations, this is known as the Schwarzchild metric. It was derived by Karl Schwarzchild while serving in the German army in WW1 and describes spacetime under the influence of a massive, non rotating and spherically symmetric object, i.e. the simplest, most fundamental case, however it will still be useful for our purposes [4]. The formula is:

$$ds^2 = -(1 - \frac{2GM}{c^2r})c^2dt^2 + (1 - \frac{2GM}{c^2r})^{-1}dr^2 + r^2d\Omega^2. \tag{1.12}$$

In the weak field limit this formula can be expanded as a Taylor series around a flat spacetime as

$$\frac{2GM}{c^2r} \ll 1,$$

this expansion yields the correction term by comparing the expanded terms in the brackets with the formula

$$1 + \frac{2\Phi}{c^2},$$

to derive the gravitational term Φ and then plugging it into the formula $F = -m\nabla\Phi$, to retrieve the Einstein correction term given above (1.11).

1.5 Chaos in Orbital Dynamics

Mercury's orbit is of particular interest in chaos studies due to its proximity to the Sun and relativistic effects, which cause a precession of 43 arcseconds per century. This precession interacts with gravitational forces from nearby planets like Venus, Earth, and Jupiter, creating a complex multi-body problem. While Mercury's orbit is stable over short timescales, numerical simulations suggest it may become chaotic over billions of years, potentially leading to erratic behaviour or collisions with the Sun, Venus, or Earth. Chaos theory highlights the sensitivity of orbits to initial conditions, where even small changes can significantly alter Mercury's path.

1.5.1 Key Concepts in Chaotic Orbital Mechanics

In chaotic systems, a small change in the starting position or velocity can lead to drastically different outcomes after a certain period. This is sometimes known as the "butterfly effect." For orbital systems, this means that tiny perturbations (like gravitational nudges from other planets or minor changes in velocity) can significantly affect a planet's path over millions of years [5].

1.5.2 Lyapunov Exponent

The Lyapunov exponent helps determine if a system is chaotic by quantifying its sensitivity to initial conditions.

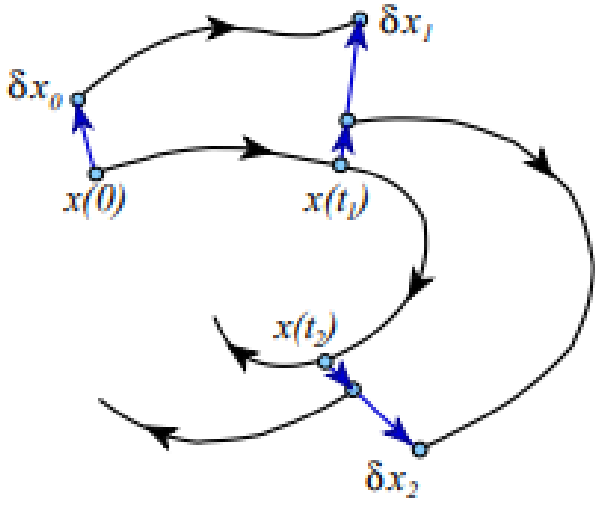

Figure 3: To compute the leading Lyapunov exponent over a long period, it's necessary to repeatedly rescale the distance between nearby trajectories to ensure their separation remains within the range where linear approximations are valid.

For a strange attractor, nearby trajectories $x(t) = f^t(x_0)$ and $x(t)+\delta x(t) = f^t(x_0+\delta x_0)$ separate exponentially with time, eventually spanning the accessible state space [6]. This behaviour is expressed as:

$$\|\delta x(t)\| \approx e^{\lambda t}\|\delta x_0\|,$$

where λ, the *leading Lyapunov exponent*, represents the mean rate of separation of trajectories. Over infinite time, λ provides a global measure of divergence, averaged over the attractor [7].

The Lyapunov exponent λ is defined as:

$$\lambda = \lim_{t\to\infty} \lim_{\Delta x(0)\to 0} \frac{1}{t} \ln \frac{\|\Delta x(t)\|}{\|\Delta x(0)\|}, \tag{1.13}$$

where:

- $\Delta x(0)$ is the initial infinitesimal separation between two nearby trajectories in the phase space.
- $\Delta x(t)$ is the separation at time t.

- $\|\cdot\|$ denotes a norm (typically the Euclidean norm).

This definition captures how small perturbations grow or shrink over time, indicating the system's sensitivity to initial conditions.

Interpretation of λ

- $\lambda > 0$: Exponential divergence of trajectories. This indicates chaos, where nearby points in phase space diverge rapidly, leading to unpredictable long-term behaviour.
- $\lambda = 0$: Neutral behaviour. The separation between trajectories neither grows nor shrinks exponentially.
- $\lambda < 0$: Exponential convergence of trajectories, indicating a stable system where perturbations decay.

1.5.3 Resonance & Perturbations

Chaos in orbits often arises due to resonances between celestial bodies. A resonance occurs when two bodies have orbital periods that are close to a ratio of small integers, which can lead to repeated gravitational interactions that amplify perturbations. In our Solar System, the gravitational influence of Mercury is a major source of resonances and perturbations for Mercury, which can drive chaotic changes in its orbit over long periods [8]. We can calculate orbital periods using the Kepler's Third Law equation (1.1).

2 Numerical Methods for Orbital Dynamics

Numerical methods, such as Euler, Leapfrog, and Runge-Kutta, provide ways to approximate the solution to ordinary differential equations (ODEs) by stepping through time in discrete intervals.

2.1 Euler's Method

Euler's method is the crudest approach to numerically solving a system of ODEs where it uses a discrete time step Δt to approximate the solution. If we are solving for $x(t)$, the position of an object in orbit, the update rule is given by:

$$x_{n+1} \approx x_n + \Delta t\, f(t_n, x_n)$$

This formula approximates the position at time t_{n+1} as a linear shift from x_n, using the derivative $f(t_n, x_n)$, which is the rate of change of x at time t_n.

For coupled ODEs, Euler's method is extended as follows:

$$x_{n+1} \approx x_n + \Delta t\, f(t_n, x_n, y_n)$$
$$y_{n+1} \approx y_n + \Delta t\, g(t_n, x_n, y_n)$$

where $f(t_n, x_n, y_n)$ and $g(t_n, x_n, y_n)$ are the functions that define the derivatives of x and y, respectively. This approach can be extended to higher-order ODEs by rewriting them as systems of first-order ODEs, as shown in the example for a second-order ODE in orbital dynamics. The Euler method is first-order accurate, meaning the global error is proportional to Δt.

2.2 Leapfrog Integration

Leapfrog integration is a second-order time-stepping method often used to solve second-order ODEs, such as those governing orbital dynamics. The key feature of this method is the use of a midpoint approximation, which improves accuracy compared to Euler's method.

Starting with the second-order ODE:

$$\frac{d^2x}{dt^2} = f(t, x)$$

We rewrite this as a system of two first-order equations:

$$\frac{dx}{dt} = v, \quad \frac{dv}{dt} = f(t, x)$$

The Leapfrog method then proceeds by updating position and velocity in a "kick-drift-kick" manner:

$$v_{n+1/2} = v_n + \frac{\Delta t}{2} f(t_n, x_n)$$

$$x_{n+1} = x_n + \Delta t \, v_{n+1/2}$$

$$v_{n+1} = v_{n+1/2} + \frac{\Delta t}{2} f(t_{n+1}, x_{n+1})$$

Leapfrog integration's simplicity, stability, and symplectic properties make it a cornerstone in computational physics, particularly for simulating systems where the interaction between position and velocity must be carefully balanced. This method is second-order accurate, meaning the global error is proportional to Δt^2.

2.3 Runge-Kutta Methods

Runge-Kutta methods are a family of one-step methods used for solving first-order ODEs. These methods improve on Euler's method by using intermediate steps to better estimate the solution. They are preferred when high accuracy is needed over short intervals or when the ODE does not exhibit oscillatory behaviour requiring long-term stability (in such cases, methods like Leapfrog are better).

The simplest Runge-Kutta method, known as the midpoint method (or RK2), uses two stages:

1. Predict a midpoint value:

$$k_1 = \Delta t \, f(t_n, x_n)$$

$$k_2 = \Delta t \, f\left(t_n + \frac{\Delta t}{2}, x_n + \frac{k_1}{2}\right)$$

2. Update the value of x_{n+1} using the predicted midpoint:

$$x_{n+1} = x_n + k_2$$

This method is second-order accurate like Leapfrog, with global error proportional to Δt^2.

The most commonly used version of Runge-Kutta is the fourth-order method (RK4), which requires four stages:

$$k_1 = \Delta t \, f(t_n, x_n)$$

$$k_2 = \Delta t \, f\left(t_n + \frac{\Delta t}{2}, x_n + \frac{k_1}{2}\right)$$

$$k_3 = \Delta t \, f\left(t_n + \frac{\Delta t}{2}, x_n + \frac{k_2}{2}\right)$$

$$k_4 = \Delta t \, f(t_n + \Delta t, x_n + k_3)$$

The final update rule is:

$$x_{n+1} = x_n + \frac{1}{6}\left(k_1 + 2k_2 + 2k_3 + k_4\right)$$

The RK4 method is fourth-order accurate, meaning its global error is proportional to Δt^4, indicating the best numerical stability.

2.4 Initial Conditions

To apply numerical methods to this orbital problem, some initial values are required. Naturally, the position of Mercury will change as it orbits the Sun, and because of the orbit's elliptical shape, so will the magnitude of the velocity.

Having the initial conditions taken at the perihelion, which can be defined to be on the same horizontal axis as the Sun, as shown in Figure 1, allows for a simpler definition of these conditions. Defining the Sun at (0,0) means that using known eccentricity (e) and semi-major axis (a) of the ellipse, the initial x position is simply $a - ea$ and the inital position of y is 0.

The x-component of the initial velocity at the perihelion is 0 because in orbital motion, the velocity is tangent to the object's path. At the perihelion in this coordinate system, Mercury has reached its turning point, where its motion is entirely along the y-direction. The y-component of the velocity at the perihelion can be derived by considering the conservation of the angular momentum and energy. Angular momentum is defined as $L = mvr$, and the total energy of the system is the sum of potential and kinetic energy; $\frac{1}{2}mv^2 + \frac{-Gm_1m_2}{r}$. Defining v_1 as the velocity at the perihelion and v_2 the velocity at the aphelion, the velocity at the aphelion can be expressed as:

$$v_2 = v_1 \frac{a - ea}{a + ea} \tag{2.1}$$

Then by applying the conservation of energy at each point, with r_1 the distance from the Sun to Mercury at the perihelion and r_2 the distance to Mercury at the aphelion, the following equation is found:

$$\frac{1}{2}m{v_1}^2 - \frac{Gm_sm_m}{r_1} = \frac{1}{2}m{v_2}^2 - \frac{Gm_sm_m}{r_2}$$

By substituting the result from the conservation of angular momentum 2.1 into this equation and rearranging, an expression for v_1 is found that depends on the mass of the Sun, the eccentricity, and the semi-major axis:

$$v_1 = \sqrt{\frac{2Gm_s(\frac{1}{a-ae} - \frac{1}{a+ae})}{1 - (\frac{a-ae}{a+ae})^2}}. \tag{2.2}$$

For Mercury, this is approximately $12.442 AU/Yr$.

3 Results

The primary focus was to model the orbit of Mercury around the Sun using different numerical integration techniques, which were then compared and also to implement General Relativity to simulate the orbits.

3.1 Comparison of Numerical Methods

Initial simulations of Mercury's orbit show a clear distinction between the numerical method used and the accuracy with which it computes an orbit. Running these numerical method functions over a larger yet reasonable amount of steps and hence shorter step size allows for a more accurate plot of the orbit.

As seen in Figure 4, while for 500 time steps Leapfrog, RK2 and RK4 are able to form a clearly accurate orbit of Mercury, Euler's method struggles to form a complete loop and is clearly not an accurate representation of Mercury's orbit. On the other hand at a higher number of steps more complete solutions are found, as seen in Figure 5.

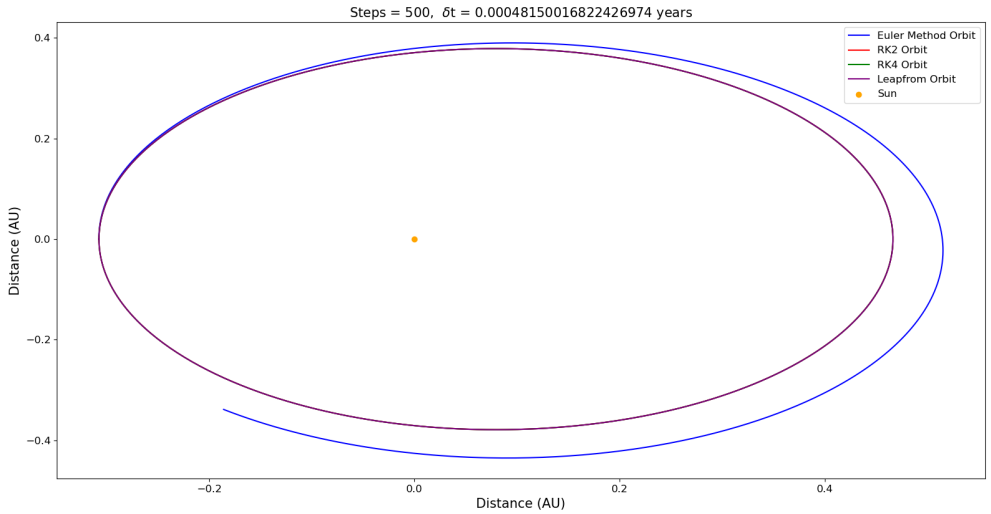

Figure 4: Orbit of Mercury around the Sun calculated using a variety of Numerical methods described in the Mathematical background over 500 time steps, for one complete orbit around the Sun.

It is clear that the Euler method has little further use for this problem, it's methodology is too basic and contains many issues that can be resolved by changing to a more complex numerical method.

Further supporting the dismissal of the Euler method for use in modelling Mercury's orbit, Figure 6 shows how the error of the Euler method is much greater than that of the RK2 and RK4 methods. It does this by quantifying the distance between the last modelled point for a fixed number of steps and the start point of the orbit defined by the initial values.

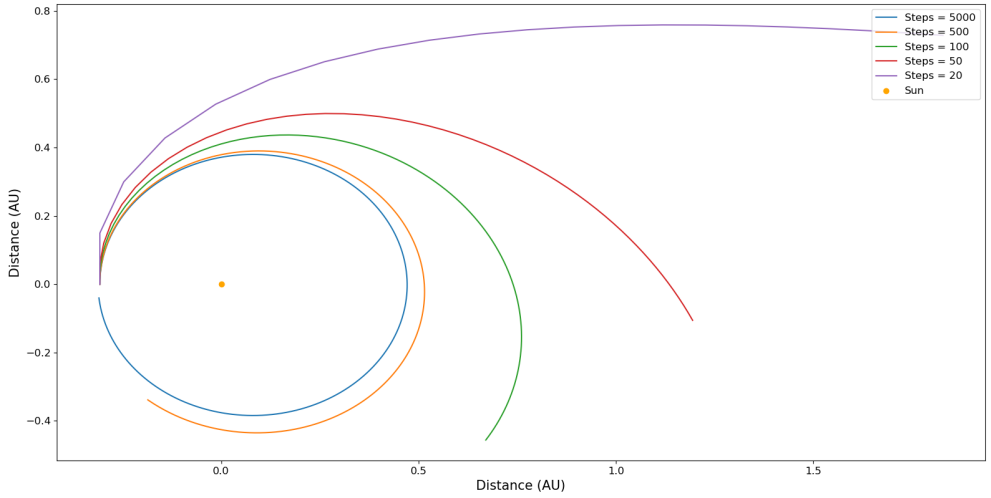

Figure 5: Plot of Steps in Euler Method, showing as the amount of steps used in the Euler method increases, the solution gets closer to a closed elliptical orbit, despite still being clearly inaccurate at 1500 steps.

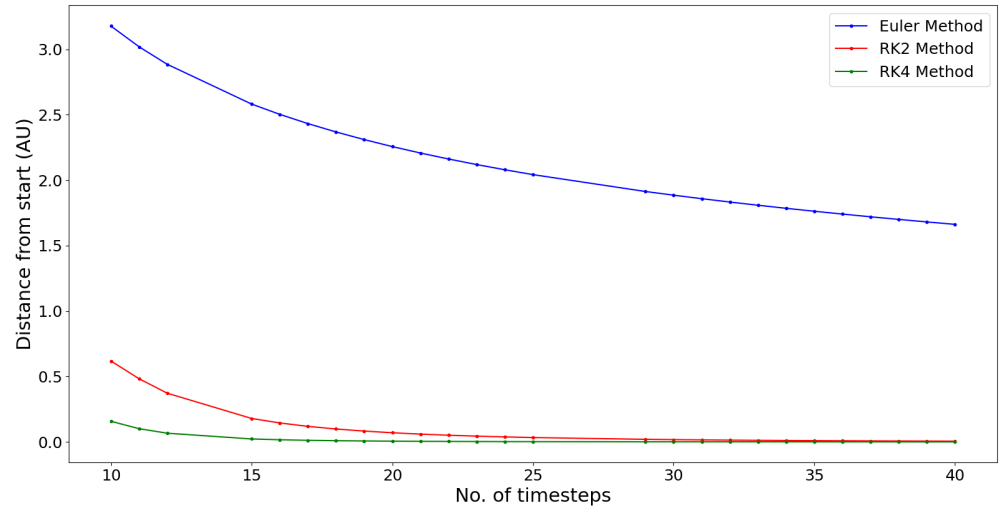

Figure 6: Plot of convergence, showing how as time step increases the distance from the end of the loop for different numerical methods changes. For each plot a few values are masked out as they were numerical outliers that had no significance.

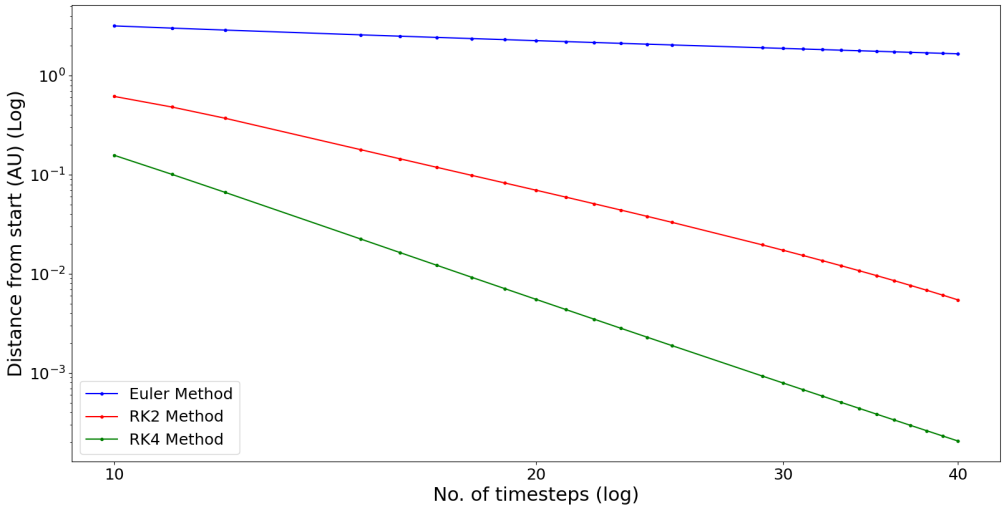

Figure 7: Plot of convergence using log-log, showing the log (base 10) graph of number of time steps against distance from initial point for different numerical methods.

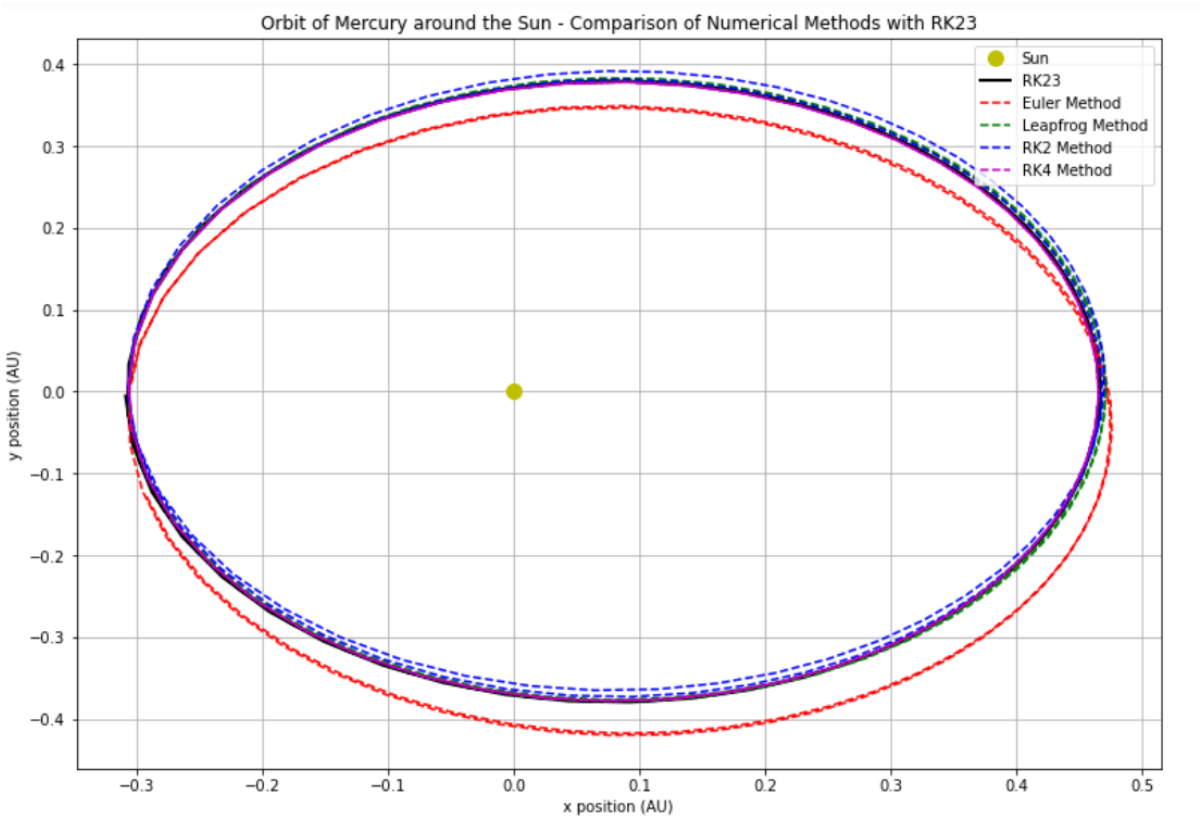

Figure 8: Plot of comparison of different Numerical Methods with RK23.

Method	Theoretical Prediction	10-50 Steps	10-100 Steps	10-300 Steps	10-1000 Steps
Euler	1	0.44	0.45	0.52	0.68
RK2	2	3.75	3.76	1.89	1.67
RK4	4	5.06	4.87	4.22	3.94

Table 1: The convergence plot is simulated over a larger range of steps (step number equals the difference in the range), the gradients of the convergence plot converge to the predicted values. For each of the step ranges, the absolute value of the gradient of the log-log plot is shown, calculated using SciPy.

Figure 7 shows that, while at low steps (10-20), the RK2 method has a noticeably greater error than RK4. However as the time step increases the distance between the start and final values converge. It is expected that at a very small time step, or a large number of steps, the global error would converge to 0. The convergence rate of each method is related to the power of Δt representing the global error and can be seen in Table 1. Here it is further supported that RK4 is more successful than the other numerical methods.

Method	Time (s)
RK23	0.009211
Euler	0.000656
Leapfrog	0.001344
RK2	0.001618
RK4	0.002898

Table 2: Time taken by different Numerical Methods.

3.2 Energy Considerations Using Runge-Kutta Integration

Using the solutions to the RK4 method for the orbit of Mercury around the sun we can determine the total energy of the system - and thus the kinetic and potential energy - against time in the scale of a full orbit. Using 1.6 to model the kinetic energy and 1.7 to model the potential energy, we simulate the orbit of Mercury around the Sun. Using solutions for the energy of the system and various positions, the kinetic and potential energy are plotted against the time advance, in the scale of one orbital period.

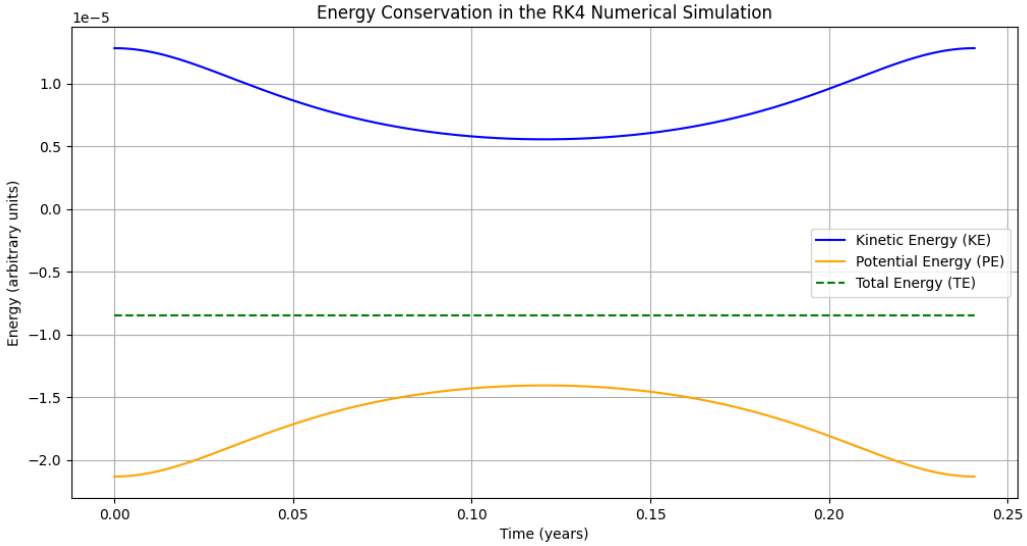

Figure 9: Kinetic energy, potential energy and total energy of Mercury plotted against time

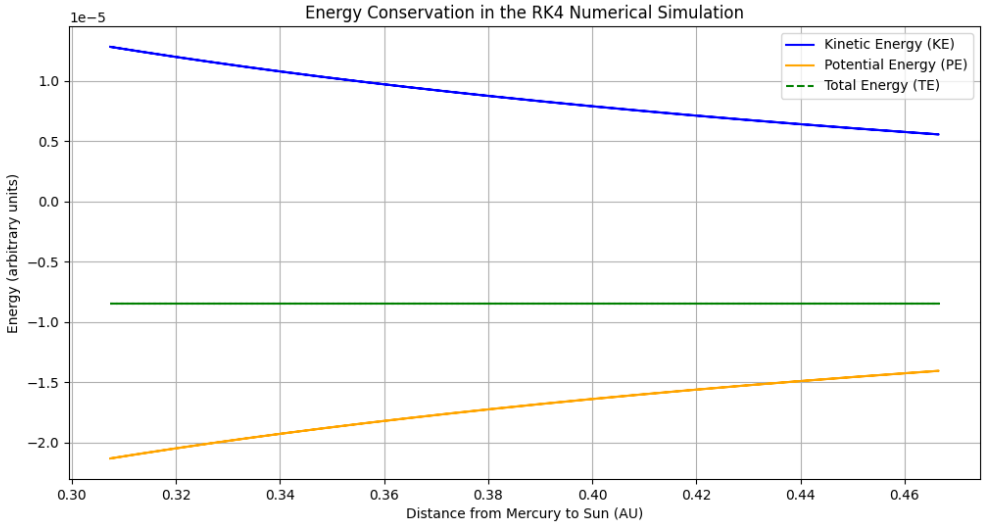

Figure 10: Kinetic energy, potential energy and total energy of Mercury plotted against distance to Sun

As seen in Figure 9 the total energy of the system is constant as proved in the derivation of 1.8 due to the energy being shown as a straight horizontal line. Kinetic energy is shown to reach its maximum at the start of the orbit where it is furthest away from the Sun - at its aphelion - as shown in Figure 10. Conversely, at the aphelion is when the potential energy is at its lowest. The potential energy is shown here as a negative value due to it being defined as the energy required to move the mass from r to infinity, where the potential is zero.

This model clearly shows that this orbital system obeys the laws of conservation of energy and total energy is constant during the period of the orbit, it is consistent in our predicted understanding of the inverse proportionality that generational potential energy has due to its $\frac{1}{r}$ term.

3.3 Simulation of Orbital Motion with General Relativity Corrections

All constants were initialised with the masses of the Sun and planets in Astronomical Units (AU), years, and solar masses for consistency. The orbital properties for the planets were defined using data collected from the NASA planetary dataset [9]. The simulation was run over one Venusian year to observe the orbital dynamics as seen in Figure 11.

The periapsis was calculated and its velocity was determined using Eq. 2.2. The relativistic equations of motion, including the GR corrections, were computed from the GR-modified equations of motion (Eq. 1.11).

The aim of including GR corrections was to capture small deviations in orbital motion caused by relativistic effects for Mercury and Venus. The equations of motion were solved numerically using the RK45 method.

As an additional challenge, the *barycentre* (centre of mass) of the two planets was calculated using the formula:

$$\text{COM} = \frac{m_1\vec{r}_1 + m_2\vec{r}_2}{m_1 + m_2} \tag{3.1}$$

where m_1, m_2 are the masses of Mercury and Venus, and $\vec{r}_1, \vec{r}_2$ are their respective position vectors. This calculation dynamically updated as the planets orbited the Sun. For further refinement, the Sun could be included in the barycentre calculation for completeness. However, its significant mass would shift the COM very close to the Sun, making small changes in the barycentre harder to observe visually.

It is observed that both Mercury and Venus exhibit an inward spiralling motion towards the Sun due to GR effects, which alter their elliptical orbits over time. The barycentre lies closer to Venus, as its larger mass dominates the system, but it also moves inward, following the trajectories of the two planets.

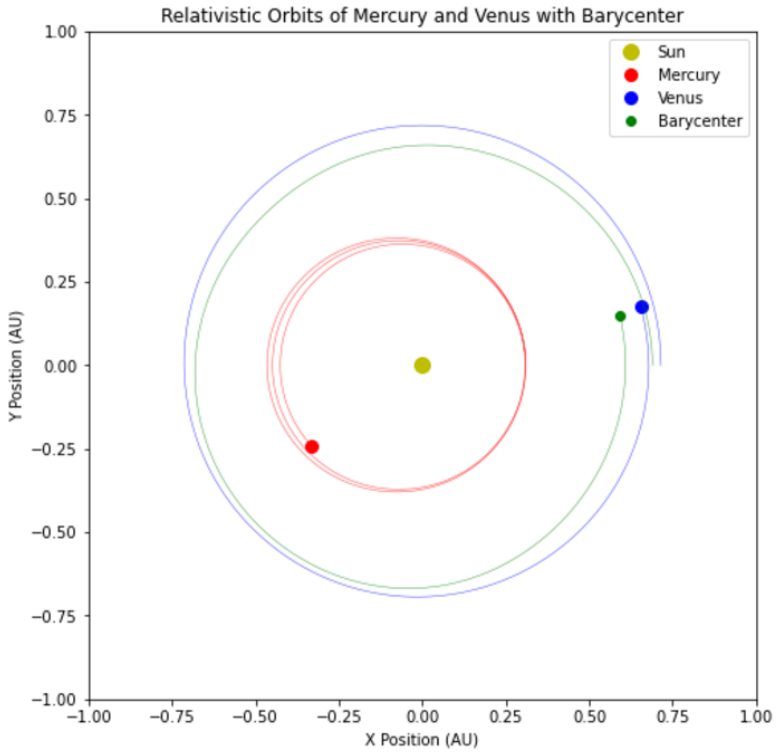

Figure 11: Animation showing the orbits of Mercury and Venus along with their barycentre.

3.4 Lyapunov Exponent & Divergence Calculation

After deriving the Lyapunov Exponent, adding a slight perturbation to Mercury's initial velocity on its orbit over the course of a year, defining two sets of initial conditions and integrating them using the `scipy.integrate.solve_ivp` function, the resulting perturbed trajectory is obtained and visualized in Figure 12.

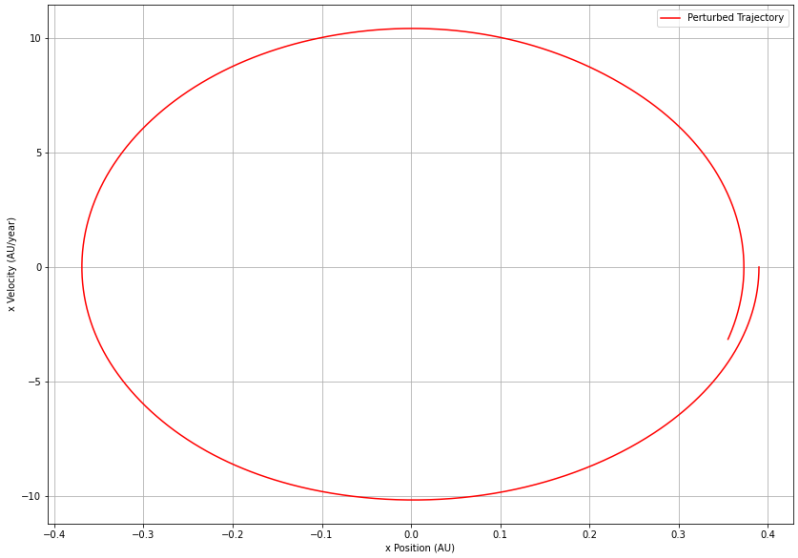

Figure 12: Shows the orbit of Mercury once introducing a small perturbation of 10^{-5} Plotting the x-component of its velocity against the x-component of its position. The estimated Lyapunov Exponent is: 19.269453 (1/year).

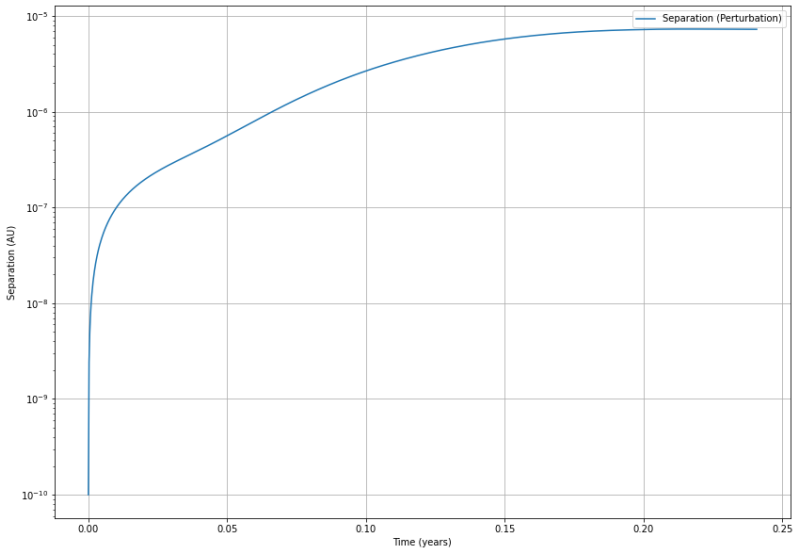

Figure 13: Demonstrates the perturbed trajectory over several orbital cycles, deviations from the unperturbed orbit may grow significantly.

The perturbed trajectory still forms an elliptical shape, consistent with the gravitational dynamics of a two-body system. Although the overall shape remains elliptical, the phase angle likely shifts, leading to a gradual divergence between the perturbed and unperturbed trajectories. While the short-term dynamics appear stable (remaining in a bounded elliptical orbit), small perturbations compound over time as showcased in Figure 13.

Such divergence can be critical when modelling planetary systems, as it affects predictions of Mercury's orbit far into the future. Despite the sensitivity, the trajectory does not escape the phase-space ellipse, indicating that the orbit remains stable. This reflects the gravitational stability of Mercury's orbit in the short to medium term, as the system is energetically constrained. The logarithmic growth of this separation further also verifies that the Lyapunov exponent should be positive.

3.5 Mercury & Venus' Orbital Resonance

In order to verify the theory behind orbital resonance, The graph in Figure 14 visualizes the orbits of Mercury (blue) and Venus (red) around the Sun (orange dot) over a simulated period of 50 years in a heliocentric coordinate system. Mercury's orbit, depicted as a smaller and more compact ellipse, demonstrates its closer proximity to the Sun and its shorter orbital period, aligning with Kepler's Third Law, which states that closer planets have faster orbits. Venus's orbit, being larger and less eccentric, reflects its greater distance from the Sun and a slower orbital period compared to Mercury.

Perturbations shown in the graph are relatively minor, showcasing the stability of their orbital resonance and the dominance of the Sun's gravitational field in maintaining their predictable motions over extended time frames. The Sun, located at the origin, serves as the focal point of both elliptical trajectories. Mercury completes one orbit around the Sun in about 0.24 years (88 Earth days), reflecting its close proximity to the Sun (0.39 AU) and high orbital velocity due to the Sun's strong gravitational pull. According to Kepler's Third Law, its short orbital period corresponds to a smaller semi-major axis, consistent with its compact, elliptical orbit. The ratio of Mercury's orbital period to Venus's (0.392) indicates Mercury completes approximately 2.55 orbits for every orbit of Venus. While not an exact resonance, this ratio highlights their dynamic interplay in the Sun's gravitational field. These values illustrate the predictable nature of planetary orbits and provide a quantitative comparison of their relative speeds and distances.

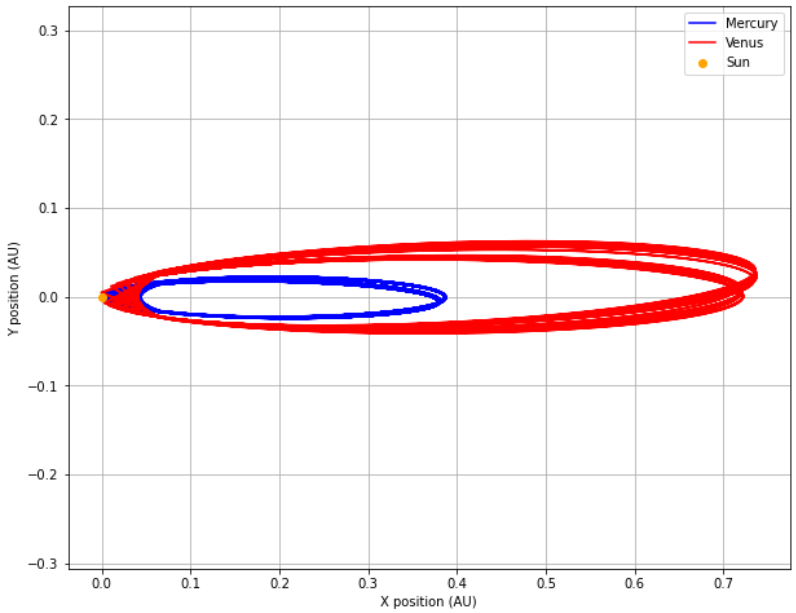

Figure 14: Shows the orbital resonance between Mercury (blue line) and Venus (red line). The simulation is run over 50 Earth years. Orbital Period of Mercury: 0.24 years, Orbital Period of Venus: 0.61 years, Ratio of periods (Mercury / Venus): 0.392.

3.6 Comparison with Observational Data

After obtaining the ephemeris data from the JPL Horizons website [9], the x-components of the position and velocity from the observational data were plotted, as shown in Figure 15.

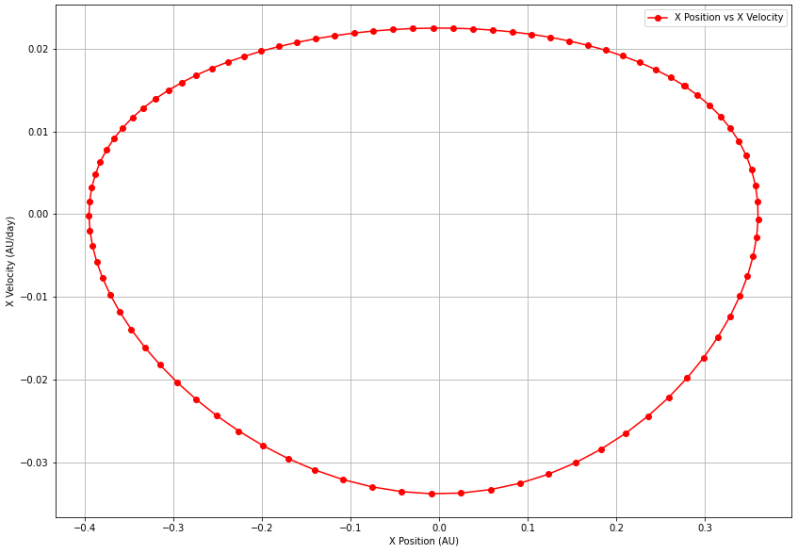

Figure 15: Shows the observational data extracted and plotted from Nov 25 2023 to Feb 21 2024 (88 days).

Figure 15 illustrates the actual trajectory of Mercury over the given time frame. The red points in the graph exhibit scatter due to:

1. Measurement inaccuracies present in real-world observational data.
2. Non-linear perturbations influencing Mercury's orbit, such as gravitational effects from other planets or relativistic corrections.

To further analyse Mercury's dynamics, the perturbed orbit from Figure 16 is an additional graph, enabling a comparison between the perturbed trajectory and the observational data. This comparison highlights deviations and provides insights into the factors affecting Mercury's orbital behaviour.

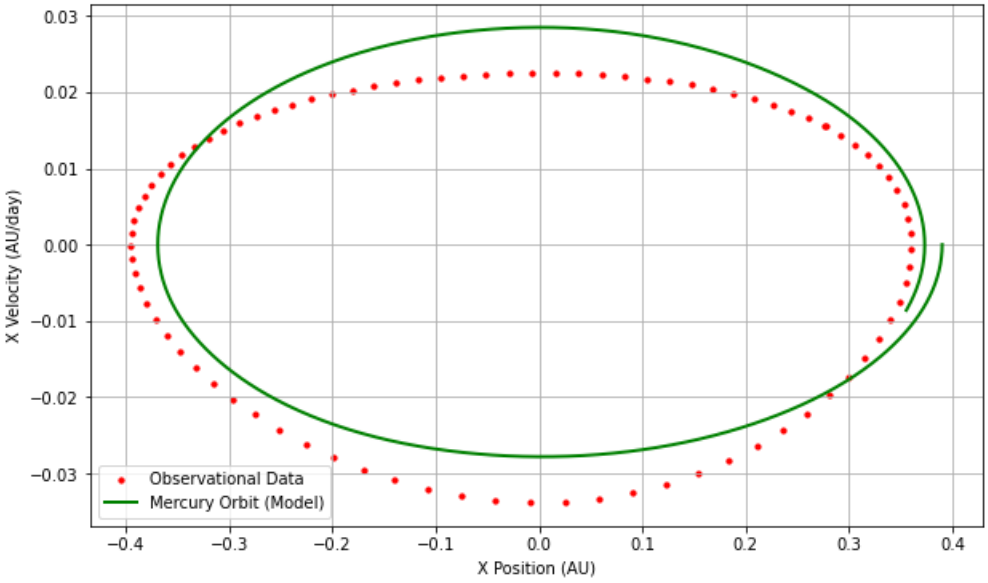

Figure 16: The x-components of the position and velocity, comparing observational data (red dots) and the perturbed trajectory (green line).

The observed data points closely follows the simulated trajectory, but small deviations are visible, particularly near the aphelion and perihelion. These deviations could arise from perturbations due to other celestial bodies or limitations in the observational precision. The elliptical shape of the graph reflects the nature of Mercury's orbit, with its velocity increasing near perihelion due to stronger gravitational acceleration from the Sun and decreasing near aphelion as it moves farther away. The agreement between the model and the data confirms the reliability of the simulation in capturing Mercury's key orbital characteristics.

3.7 Difficulties faced

During the Lyapunov Exponent calculation, an issue was face of dealing with log(0); which was resolved by introducing a threshold, 10^{10} to prevent zero separation, and the logarithmic function was modified to $\log(x + \epsilon)$ for numerical stability. For the orbital resonance graph, Venus' mass was amplified to highlight its gravitational effects. The main challenge, however, was processing observed Ephemeris data, due to differences in units and format, demanding custom code to convert it for comparison with the theoretical model.

4 Conclusions

Modelling the orbit of planets in our solar system required the use of numerical modelling, theoretical analysis, and comparisons with observational data to provide an understanding of orbital dynamics and Kepler's Laws. Through this study numerical methods such as Euler's, Runge-Kutta, and Leapfrog were used to estimate solutions to Kepler's Laws, with higher-order methods proving both more accurate and efficient, with Figure 4 clearly showing that higher order numerical methods produce a more elliptical orbit.

The inclusion of relativistic corrections shows the limitations of Newtonian orbital mechanics in accurately describing Mercury's perihelion precession. Observational data lead many to believe that Mercury's orbit is not stable and its perihelion advance cannot be explained by Newtonian mechanics, this was accounted for via a non-trivial solution in the form of equation 1.11.

The study of chaotic dynamics via the Lyapunov exponent showcased how small changes in the velocity of the orbit of Mercury can have exponentially increasing effects on the size of the planets orbit, as shown by Figure 13. The graph levels off over time becoming a stable orbit at a constant separation from the Sun. The perpetuated initial conditions still yields a stable orbit and consistent orbital shape in the short to medium term.

In conclusion, this project highlights the interplay between Classical Mechanics, Relativity, and Chaos theory in understanding orbital systems, such as Kepler's Law. It also emphasizes the value of computational methods in discovering the outcomes of planetary dynamics, paving the way for further exploration of multi-body interactions and long-term orbital predictions.

A Python Code

All python code has been uploaded to a GitHub repository. Along with the group associated OneDrive set up by Greg Ashton.

B Author Contribution

Harry Nsubuga contributed to the project by developing the code for the Runge-Kutta 2 numerical method. Harry also implemented and generated code and plots for the Lyapunov Exponent, orbital resonance, and the comparison with observational data, as well as authored the corresponding sections in the report.

Shreya Ghosh authored the methods section of the report, computed the Leapfrog algorithm, compared all the Numerical Methods with RK23 along with their efficiencies and coded an animation of Mercury, Venus and their COM as discussed in the report.

Oliver Blease contributed by working on the initial model of Mercury and Venus's coupled orbit, coded the relationships between different numerical methods and wrote parts of the report including initial values and parts of the comparison of numerical methods.

Thomas Mansfield developed the code for the Runge Kutta 4, the code for adding the general relativistic correction term and researched into the mathematical derivation of these terms to help write up the section of the report on General Relativity.

Carolena Lukaszek performed a method for comparison, coding a log-log plot for all the different methods to showcase which is most effective in demonstrating the orbit for Mercury. Report wise, the write up for the abstract and mathematical section was done, and the general overseeing for the final draft, keeping it consistent.

Alex Boxer developed the code for the visualisation of data using a shiny app in python. Derived equations used to produce energy considerations for the two body Mercury-Sun orbital system, where results were then plotted and discussed in the report, and the write up for the conclusion.

References

[1] *Orbits and Kepler's Laws, NASA Science Kepler's Laws*. Accessed November 8 2024, from https://science.nasa.gov/solar-system/orbits-and-keplers-laws/

[2] *Kepler's Laws*. Accessed November 8 2024, from http://hyperphysics.phy-astr.gsu.edu/hbase/kepler.html

[3] *Celestial mechanics - Newton's derivation of Kepler's Laws*. Accessed November 15 2024, from https://vikdhillon.staff.shef.ac.uk/teaching/phy105/celsphere/phy105_derivation.html#:~:text=r1%20%3D%20m2a,m1%20%3E%3E%20m2

[4] *Schwarzschild Solution to Einstein's General Relativity*. Accessed November 15 2024, from https://sites.math.washington.edu/~morrow/336_20/papers17/carson.pdf

[5] *Orbital Resonance in Planetary Systems*. Accessed November 17 2024, from https://www.eolss.net/Sample-Chapters/C01/E6-119-55-12.pdf

[6] Cvitanović P., Artuso R., Mainieri R., Tanner G. and Vattay G. *Chaos: Classical and Quantum* Niels Bohr Institute, Copenhagen 2005.

[7] T.H. Author and A. Otherauthor, Chapter 'A6 Lyapunov Exponent', in P. Cvitanović, R. Artuso, R. Mainieri, G. Tanner and G. Vattay, *Chaos: Classical and Quantum*, `ChaosBook.org/version16` (Niels Bohr Institute, Copenhagen 2020).

[8] *Orbital Resonances and Chaos in the Solar System*. Accessed November 17 2024, from https://www.lpl.arizona.edu/~renu/malhotra_preprints/rio97.pdf

[9] *Approximate Positions of the Planets, NASA*. Accessed November 8, 2024, from https://ssd.jpl.nasa.gov/planets/approx_pos.html